Geomechanics and Engineering, *Vol. 43, No. 5 (2025) 379-390*
https://doi.org/10.12989/gae.2025.43.5.379

Nonlinear dynamic behavior and basin edge effect in the clayey basins under simultaneous P and SV incident waves

Hadi Khanbabazadeh*

Engineering Faculty, Gebze Technical University, 41400 Gebze, Kocaeli, Turkey

(*Received August 14, 2025, Revised November 5, 2025, Accepted November 13, 2025*)

Abstract. In the estimation of the design spectrum for sites with topographic irregularity, the instructions of the earthquake codes are to use the horizontal components of the motions. Although this approximation remains conservative for horizontally layered conditions, the effect of the P wave component at basins with 2D/3D bedrock geometry, due to the complicated interaction among different wave types, would affect the basin amplification behavior. The major contribution of this study is to present a quantitative ratio in terms of amplification factor for comparison between the simultaneous P+SV and only SV incident wave condition. To attain this goal, a fully nonlinear analysis method capable of simultaneously application of the P and SV incident motions in time domain is utilized. In this study, the effect of parameters such as clay type and basin depth is investigated. The results show the effect of the P+SV cases on the frequency content of the surface response with respect to the only SV case. It was seen that for the basin with 50m depth the aggravating effect of the P+SV incident wave remains under 20% for both soft and stiff clay types. This ratio reaches to 25% for 100 m depth basins. Along with the aggravating effect, the results show a 10% to 20% suppressive effect of the P+SV especially at basins' center with dominant 1D behavior.

Keywords: amplification factor; basin edge effect; dynamic behavior; in-plane waves; nonlinear analysis; numerical modeling; simultaneous P and SV wave's effect

1. Introduction

During an earthquake motion, the interaction among reflected and refracted waves from basin bottom and edges as well as progressive surface waves yields the 2D/3D behavior of a basin. The interference and mixing of different frequency components of the wave kinds, exist simultaneously in the half space, give rise to a complicate behavior. As a result, the surface points undergo different strain levels that would result in nonlinear behavior.

In geotechnical earthquake engineering literature, site amplification is generally defined as the differences between horizontal ground motions of two nearby sites (Anbazhagan *et al.* 2011, Roy and Sahu 2012, Saffarian and Bagheripour 2014, Shiuly *et al.* 2015). In the numerical investigations, because of its greater single effect, the used source motion type is generally shear wave (Iyisan and Khanbabazadeh 2013, Jakka *et al.* 2015, Madiai *et al.* 2016, Griffiths *et al.* 2016, Zhu *et al.* 2018, Silahtar and Kanbur 2021). Although the applied shear wave can be converted to compressional wave because of reflection and refraction in 2D basins, the complicated interaction among wave kinds give rise to the question of the coupled effect of P and SV waves when simultaneously propagated from the source.

There are several studies on the separate effect of the P and SV waves on the 2D behavior of the basins (Semblat 2011, Khanbabazadeh and Iyisan 2014a, b, Zhenning *et al.* 2020, Jianwen *et al.* 2021, Sreejava *et al.* 2023). Nevertheless, there are few studies on the coupled effect of different wave kinds on amplification behavior. It is primarily related to the difficulty of the modeling of the propagation of both shear and compressional waves together in a single model in time domain. In such studies, in addition to the response of the continua to the combined effect of both components, the definition of the motion source for the simultaneous application of the shear and compressional wave time histories in time domain must be considered properly.

Learned lessons from the different damage patterns during past earthquakes indicate the responsibility of the complicated wave interaction because of the surface and subsurface heterogeneity in alluvial basins (Kamiyama and Satoh 2002, Bakir *et al*. 2002, Pitplakis 2004, Makra *et al.* 2005, Ayoubi *et al.* 2021, Khanbabazadeh *et al.* 2016, 2019, Kumar *et al.* 2021, Ozaslan *et al.* 2022). Analytical methods remain short for the modeling of the wave transmission problems in half space. Because of the costs of the field experiments, application of the numerical methods is the most effective way of such investigations. Different numerical methods have been used for the approximation of the wave propagation in continuous layered media. The purpose of these applications is generally the modeling of the out of plane SH and/or in-plane P-SV waves. Successful application of finite element, finite difference, boundary element including DBEM and IBEM, spectral element, mesh-free and hybrid methods have been published by the researchers (Kamalian *et al.* 2006, Alielahi and Rahimi 2025, Shani-Kadmiel *et al.* 2012, Zhu and Thambiratnam 2016, Khoshghalb *et al.* 2020, Sonmezer and Celiker 2020,

*Corresponding author, Associate Professor
E-mail: hk.babazadeh@gtu.edu.tr

Copyright © 2025 Techno-Press, Ltd.

ISSN: 2005-307X (Print), 2092-6219 (Online)

Salehi *et al.* 2022, Bordoni *et al.* 2023, Shafee and Khoshghalb 2021, 2022).

Because of the significant effect of topography and layering, the effect of focusing, mode conversion and frequency dependent amplification cannot be seen in the traditional 1D approximations (Roy and Sahu 2012, Abraham *et al.* 2015, Madiai *et al.* 2017, Sonmezer *et al.* 2018). To have a better estimation of the field condition, 2D and 3D approximation of the alluvial basins are considered in the investigations (Makra and Chavez-Garcia 2016, Yniesta *et al.* 2017, Stanko *et al.* 2019, Mayoral *et al.* 2019, Rodriguez *et al.* 2021, Khanbabazadeh 2024). Several attempts have been done to correlate the results of simple 1D analyses with 2D and 3D results (Manakou *et al.* 2010, Stamati *et al.* 2016, Hasal *et al.* 2018, Saenz *et al.* 2019). Also, the use of wavelets as the dynamic motion is common in the local site effect and wave scattering studies (Alielahi and Adampira 2018). Although the general basin behavior can be figure out using such pulses, the amplification behavior of the basin can be better quantified under real strong ground motions with random nature in time domain.

Although the majority of the studies consider the separate wave type effect, there are examples of the simultaneous application of P and SV waves in a single model (Vireux 1986, Cao and Greenhalgh 1992, Oral *et al.* 2023). Main difference of such 2D application is the definition of the in-plane P and SV wave components at the same node. Oral *et al.* (2023) suggests the use of multidimensional modelling because of the resulted larger deformations under this complex wave field.

The coupling effect of the P and SV waves gets generally more important when the interaction among waves determines the amplification behavior of the 2D basins. In this study, a finite difference based fully nonlinear method that considers both shear and compressional waves together in a single simulation is applied. This feature plays important role in the better modeling of the surface wave formation and the interaction among wave types existing in the half-space. Through the assignment of nonlinear material law, the modeled continua respond to the combined effect of both wave components. Also, the interference and mixing of different frequency components occur naturally in time domain. In this way, the amplification behavior of clayey basins under simultaneous P-SV waves and SV wave will be compared. The basin models will be subjected to the components of real earthquakes scaled to a target spectrum. To make the results useful in engineering practice, the spectral amplification of basins with two depths as well as two soft and stiff clays with respect to the soil classification codes are presented.

2. Analysis method

The critical point of the simultaneous application of P and SV waves is definition of two separate in-plane wave types at the same node. To do that, the bottom boundary nodes should be able to introduce the shear and compressional effects separately. In this method, the local coordinate of a boundary grid point is defined by a right handed coordinate system composed of dip, strike and normal directions. The normal direction vector is the average normal vector of the faces meeting at the grid point, as shown in Fig. 1. For cubic boundary element that nodes aligned in horizontal direction the normal vector will be in vertical direction.

2.1 Motion equations of the nodal points

A mass point in the Lagrangian formulation is characterized by displacement, velocity and acceleration vector components. The stress state at a given node is defined by the stress tensor σ_{ij}. Using Cauchy's formula, the traction vector [t] on a face with unit normal [n] can be presented by

$$t_i = \sigma_{ij} n_j \tag{1}$$

Also, rate of strain and rotation for a point moving with velocity [v] can be characterized by

$$\xi_{ij} = \frac{1}{2}(v_{i,j} + v_{j,i}) \tag{2}$$

$$\Omega_i = -\frac{1}{2} e_{ijk} \omega_{jk} \tag{3}$$

Where ξ_{ij}, Ω_{ij} and e_{ijk} are the strain-rate tensor, rotation with angular velocity and permutation symbol, respectively. The components of the rate of rotation tensor [ω] is presented by

$$\omega_{ij} = \frac{1}{2}(v_{i,j} - v_{j,i}) \tag{4}$$

Through the application of the continuum form of the momentum principle, Cauchy's equations of motion is written as the following

$$\sigma_{ij,j} + \rho b_i = \rho \frac{dv_i}{dt} \tag{5}$$

where ρ is the unit mass, [b] is the body force per unit mass, and $d[v]/dt$ is the acceleration.

The preceding equations along with constitutive relations give the behavior of the considered material. Considering the history of loading of a frictional material (k), the constitutive equation is given by

$$[\breve{\sigma}] = H_{ij}(\sigma_{ij}, \xi_{ij}, \kappa) \tag{6}$$

where [$\breve{\sigma}$] is the co-rotational stress rate tensor and [H] is a given function.

In the finite difference approach applied in this study, through the assumption of linear variations of the variable over finite space and time intervals, the first order space and time derivatives of a variable are approximated. In this method, the mass points of the continua are considered at the vertices of the discretized medium. They interact inside the framework of constant strain rate elements.

To derive the nodal formulation of the equations of motion, first the finite difference formulation of the tetrahedron elements should be presented. Through the application of the Gauss divergence theorem and taking

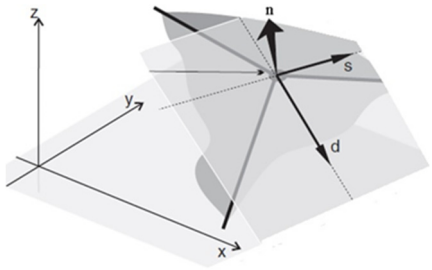

Fig. 1 Schematic presentation of the P and SV separate definition in the model bottom

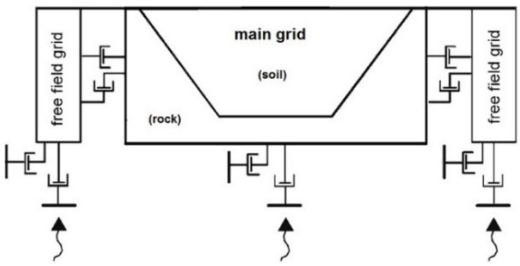

Fig. 2 Schematic presentation of the interaction between main grid and coupling boundary conditions

integrals over the volume and the surface of the tetrahedron yields

$$\int_V v_{i,j} dV = \int_S v_i n_j dS \tag{7}$$

The integration yields

$$V v_{i,j} = \sum_{f=1}^{4} \bar{v}_i^{(f)} n_j^{(f)} S^{(f)} \tag{8}$$

In this integral $\bar{v}_i$ is the average value of the velocity component i.

Considering a linear velocity variation as well as dividing by V then reorganizing terms by node contribution, the components of the strain-rate tensor is given by

$$\xi_{ij} = -\frac{1}{6V} \sum_{l=1}^{4} \left(v_i^l n_j^{(l)} + v_j^l n_i^{(l)} \right) S^{(l)} \tag{9}$$

The nodal formulation of the equations of motion are derived by application of the theorem of virtual work. By application of a virtual nodal velocity $\delta[v]^n$, the rate of the external work due to the nodal forces $[f]^n$ and body forces $[B]$ are equated with the rate of the internal work due to the stresses σ_{ij} under this velocity. Thus, the external and internal work rates are presented by the following expressions, respectively:

$$E = \sum_{n=1}^{4} \delta\, v_i^n f_i^n + \int_V \delta\, v_i B_i \, dV \tag{10}$$

$$I = \int_V \delta\, \xi_{ij} \sigma_{ij} \, dV \tag{11}$$

Finally, the external work rate may be expressed by

$$E = \sum_{n=1}^{4} \delta v_i^n [f_i^n + \frac{\rho b_i V}{4} - \int_V \rho\, N^n \frac{dv_i}{dt} dV] \tag{12}$$

where N^n is a linear function of the form

$$N^n = c_0^n + c_1^n x_1' + c_2^n x_2' + c_3^n x_3' \qquad n = 1 \; to \; 4 \tag{13}$$

2.2 Boundary conditions

In this formulation, the compressional and shear components of the incident motion are applied to each boundary nodes at each time step in time domain. Also, to consider the impedance effect, the incident motion should be applied to the underlying bedrock layer. To attain this goal, the flexible base boundary condition is applied at the bottom of the basin models. The application of the compressional and shear components independently in the normal and dip directions at the bottom boundary are as follows

$$t_n = -\rho . C_p . v_n \tag{14}$$

$$t_s = -\rho . C_s . v_s \tag{15}$$

In these equations, ρ denotes mass density. v_n and vs are components of the normal and shear velocity at the boundary, respectively. C_p and C_s are the compressional and shear wave velocity of the bottom transition layer that the incident motion is applied.

Also, to account for the nonreflecting free-field behavior at the model sides, the unbalanced force of the vertical boundary grids is estimated in parallel with the main-grid analysis. They are suppressed by the application of a similar force but in the opposite direction at each point in time domain. Fig. 2 presents the schematic presentation of the interaction between main grid and coupling boundary conditions. The estimation of the unbalanced forces is done by the following equations:

$$F_x = -\rho C_p (v_x^m - v_x^{ff}) A + F_x^{ff} \tag{16}$$

$$F_y = -\rho C_p (v_y^m - v_y^{ff}) A + F_y^{ff} \tag{17}$$

$$F_z = -\rho C_p (v_z^m - v_z^{ff}) A + F_z^{ff} \tag{18}$$

Where ρ denotes the material density along the vertical model boundary and A is the influence area of the free-field grid-point. C_p and C_s are the p and s-wave speed at the side boundary, respectively. The denotations of the other parameters are as follow:

v_x^m, v_y^m, v_z^m = x, y and z grid-point velocity in the main grid at side boundary;

$v_x^{ff}, v_y^{ff}, v_z^{ff}$ = x, y and z grid-point velocity in the side free-field;

$F_x^{ff}, F_y^{ff}, F_z^{ff}$ = free-field grid-point force with contributions from, and stresses of the free-field zones around the grid-point;

2.3 Fully nonlinear analysis method (FNM)

In this method, through the application of the explicit finite difference scheme, full dynamic equations of motions are solved in time domain. After installation of the initial stresses and forces, new velocities and displacements are estimated at each time step. Then, at every cycle, while the strain rates are calculated from the velocities, the new stresses are derived from strain rates. To secure the numerical stability, the utilized time step must be smaller than a critical value. The time step is 10e5. Since no matrices are formed in the explicit Lagrangian method, the response of the continua to large strains are calculated in reasonable computing effect. Also, despite FEM based codes, the constitutive models are considered with no adjustment to the solution algorithm. An elastoplastic soil model with failure envelope of the Mohr-Coulomb criteria has been used. The position of a stress point on this envelope is controlled by a non-associated flow rule for shear failure, and an associated rule for tension failure. To model wave transmission with more detail, the model should be discretized to elements smaller than one-tenth to one-eighth of the wave length associated with the highest Frequency component of the waves. For effective mesh scheme, the specification of both the wave-speed characteristics of the half space and the frequency content of the input motion must be considered. For this set of analyses, the mesh size has been considered as 1 m.

2.4 Damping and material properties

As known, the nature of the damping in soil is hysteresis. To apply such frequency independent damping scheme, combination of Hardin/Drnevich hysteresis damping (for elastoplastic range) along with Mohr-Coulomb model (for plastic range) have been applied. The scheme is implemented through the introduction of the modulus reduction curves by certain functions. In this way, the proper damping with respect to the stress and strain level of each mass point is applied in time domain. The geotechnical specifications of the used two clayey soils and their corresponding G/G_{max} curves are presented in Table 1 and Fig. 3, respectively. In the applied models, the variation of the soil parameters with depths has been considered as well. The correlation used to extract the modulus reduction curves is as follows

$$G_{sec}/G_{max} = A(\gamma, PI) \times \sigma_0'^{n(\gamma,PI)-n_0} \quad (19)$$

$$A = 0.5\left\{1+\tanh\left[\ln\left(\frac{0.000102+m(PI)}{\gamma}\right)^{0.492}\right]\right\} \quad (20)$$

$$m(PI) \rightarrow \begin{cases} 0.00 & PI = 0 \\ 3.37\times10^{-6}\,PI^{1.404} & 0 < PI \le 15 \\ 7.00\times10^{-7}\,PI^{1.976} & 15 < PI \le 70 \\ 2.70\times10^{-5}\,PI^{1.115} & PI > 70 \end{cases} \quad (21)$$

The parameters of these relations are shear strain level (γ), soil plasticity index (PI) and consolidation stress, σ_0'.

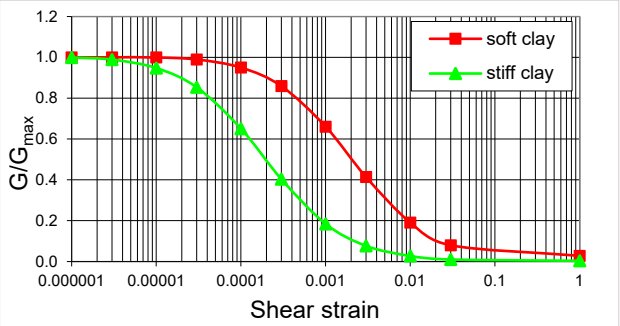

Fig. 3 Modulus reduction curves of the used soil materials in the nonlinear analysis

Table 1 Geotechnical properties of the basin clay types

Soil classification		ϕ(°)	cu (kPa)	G (MPa)	K (MPa)	γ (kN/m^3)
Clay	Soft	10	34-35	10.1-61.2	39.1-177.3	18-20
	Stiff	10	150-165	400-900	1240-2680	20-21.5
Bedrock		*	*	2200	3600	22

ϕ: internal friction angle; cu: undrained shear strength; G: shear modulus; K: bulk modulus; γ: unit weight

The linearity of G/G_{max}-γ increases with increasing σ_0'.

2.5 Model specifications and earthquake motions

General geometry of the large number of the real shallow basins can be approximated by a trapezoidal shape with varying depth of 50 m to 150 m (Semblat *et al.* 2002, Zhu *et al.* 2018, Khanbabazadeh 2024) and 5° to 15° basin edge inclination (Semblat *et al.* 2000, Khanbabazadeh *et al.* 2016, 2019, Ozaslan *et al.* 2022). The greater reflection/refraction effect of the smaller basin edge angles on the surface behavior of the 2D basins have been seen in the past studies (Semblat *et al.* 2000, Ozaslan *et al.* 2022). Thus, to increase the practical value of the study, the dynamic response of two shallow trapezoidal basins with 50m and 100m depths with 10° basin edge inclination have been selected, as shown in Fig. 4. Unlike random discretization methods, FLAC3D presents different primitives for generation of the finial discretized shape of the continua. In this study, for the basin edges, a combination of two regularly discretized wedge primitives has been used. For this, one of the wedges has been assembled on the top of the other through the correction of its internal local axes. As a result, a smooth plane for the incidence of the bedrock motion at the basin edges is provided. This meshing scheme is completed by a regularly discretized brick primitive for the internal part of the basin. As a results, the proper application and progression of the P and SV waves is provided. Since the refracted waves from the inclined bedrock as well the generated progressive surface waves would affect farther distances from the outcrop, the width of the models have been taken large enough (2000 m) for considering such effects, too.

The modeled clayey basins are subjected to a set of 24 real earthquake motions scaled to DD2 strength level with respect to Turkish seismic code provisions, corresponding

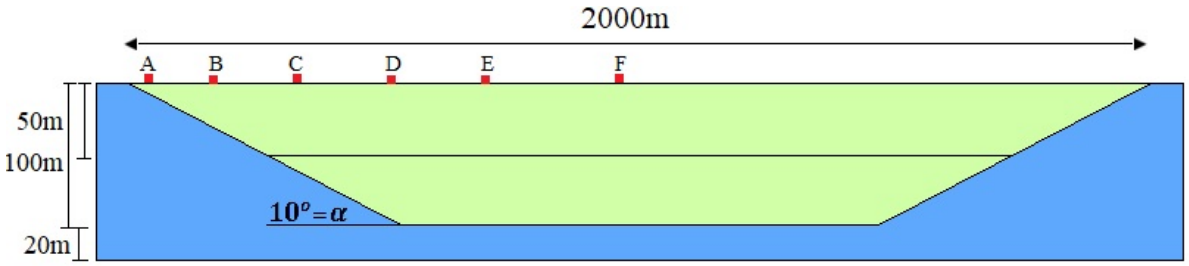

Fig. 4 Specification of the investigated 2D clayey basins and bedrock geometry

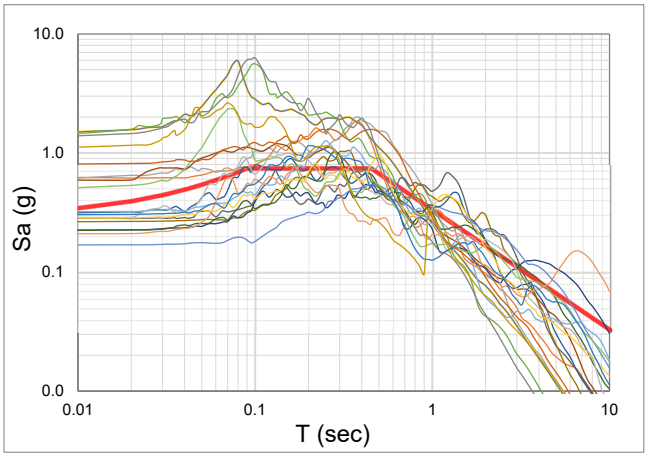

Fig. 5 Response spectra of the used strong ground motion collection scaled to target spectrum

Table 2 Specifications of the used strong ground motions

	Earthquakes	Station	Amax (g)	Magnitude	R_{JB} (km)	Arias Intensity (m/s)
1	Tottori_ Japan (10.06.2000)	OKYH07	0.1	Mw=6.61	15.23	0.3
2	Kocaeli_Turkey (17.08.1999)	Gebze	0.1	Mw=7.51	7.57	0.5
3	Mammoth lakes (25.05.1980)	USC McGee Creek	0.1	Mw=6.0	6.68	0.1
4	Anza (25.02.1980)	Pinyon Flat	0.1	Mw=5.19	12.24	0.0218
5	Palm springs1986	Silent Valley	0.1	ML=5.9	19.5	0.1
6	Chalfant (21.07.1986)	Long Valley Dam	0.1	Mw=6.2	14.97	0.2
7	Sakarya (11.11.1999)	Development bureau	0.2	Md=5.7	17.5	0.1397
8	Dinar (01.10.1995)	Dinar station	0.2	ML=5	2	0.8096
9	Duzce (12.11.1999)	Lamont-531	0.2	Mw=7.1	11.4	0.5283
10	Cape Mendocino (RSN-3744) (1992)	Bunker Hill FAA	0.2	Mw=7.01	8.49	0.6
11	Tottori_ Japan (10.06.2000	SMNH10	0.2	Mw=6.61	15.58	0.5
12	Parkfield-02_ CA (28.09.2004)	Turkey Flat#1(0M)	0.2	Mw=6	4.66	0.2
13	Mendocino 1992	EEL River valley	0.3	ML=6.5	15	0.8079
14	Coyote lake (06.08.1979)	Coyote Lake Dam	0.3	Mw=5.7	1.6	0.4003
15	Parkfield (28.06.1966)	Temblor pre	0.3	Mw=6.1	16.1	0.3615
16	Firuzabad 20.06.1994	Firuzabad-ZRT	0.3	Mw=5.9	21	0.687
17	Kobe_ Japan (16.01.1995)	Kobe University	0.3	Mw=6.9	0.9	1.2
18	Hector Mine (16.10.1999)	Hector	0.3	Mw=7.13	10.35	1.9
19	Kocaeli1 (RSN-1165) (07.08.1999)	Izmit	0.4	Mw=7.51	3.62	0.8
20	Parkfield (28.06.1996)	Temblorpre	0.4	Mw=6.1	16.1	0.5537
21	UmbriaMarche (10.16.1997)	Colfiorito-Casermette	0.4	Mw=4.3	1	0.6902
22	South Iceland (17.06.2000)	Thjorsarbru	0.4	Mw=6.5	15	1.6125
23	Manjil_Iran (20.06.1990)	Abbar	0.4	Mw=7.37	12.55	7.5
24	RSN9071-AZPFOHL(12.06.2005)	Pinon Flats Observatory	0.4	Mw=5.2	12.82	0.3

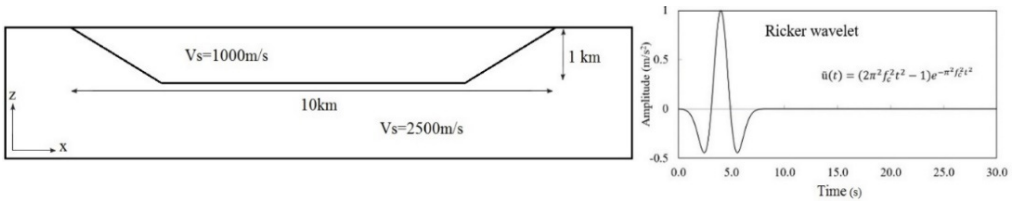

Fig. 6 Specification of the verification model and used input motion for verification

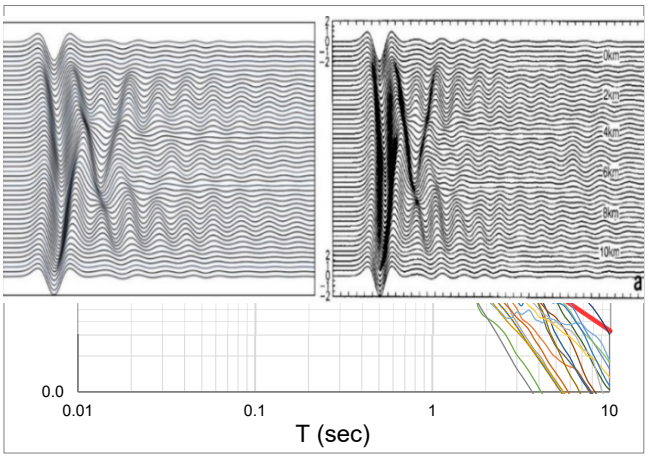

Fig. 7 Comparison between the results: Zhu and Thambiratnam (2016), Gil-Zepeda (2003) results (left), the verification model (right)

to probability of exceedance of 10 % in 50 years (with return period of 475 years). The list of the used strong motions as well as the corresponding scaled spectra are presented in Table 2 and Fig. 5, respectively. The used collection consists of motions with different specifications such as frequency content and duration. They are recorded on the rock or rock type site with shear wave velocity greater than 750 m/s, or de-convoluted to the bedrock motion using corresponding site specification. In the P+SV analyses codes, the corresponding P component of the scaled SV motion is simultaneously applied from the flexible base bottom boundary condition.

2.6 Verification

The numerical analyses of this study is applied by a finite difference base FLAC code (Fast Lagrangian Analysis of Contonua) (Cundall 2016). The verification of the applied modeling has been done by the results of the trapezoidal basin response to the Ricker pulse (Gil-Zepeda *et al*. 2003, Zhu and Thambiratnam 2016). The specification of the applied dynamic motion as well as basin geometry are presented in Fig. 6. The comparison of the time domain surface displacements in Fig. 7 shows the satisfactory crossness of the results.

3. Results and discussion

To see the quantitative effect of the combined P+SV wave propagation on the spectral amplification, first the behavior of a shallow soft clayey basin (50 m depth) under two strong motions with different frequency contents is presented. Then, to neglect to motion dependency of the results, the average response of the basin to 24 motions with different duration, frequency content, strength etc. scaled to a target spectrum will be presented. Also, the effect of the parameters such as basin depth and clay type will be discussed too. All cases are evaluated by Simultaneous Wave Effect (SWE) ratio, which is defined as the ratio of the Maximum Spectral Amplification ratio (MSAF) under P+SV to SV incident waves conditions. "*To estimate SWE Ratio and MSAF, first the acceleration responses of the surface points are recorded during time domain analyses under each twenty-four earthquake motions separately for both P+SV and SV cases. After estimation of the spectral acceleration response of each point, the spectral amplification factor with respect to the reference rock site at each period is estimated. In this stage, for each surface point the average of resulted spectral amplifications under twenty-four earthquakes are estimated. The maximums of these curves are reported as the MSAF (Maximum Spectral Amplification ratio). Finally, SWE (Simultaneous Wave Effect) is defined as the ratio of MSAF under P+SV to SV incident waves conditions.*"

3.1 Effect of the simultaneous P+SV wave on basin response

Fig. 8 shows the response spectra of two earthquakes (motions RNS1165 (Case 1) and RNS3744 (case 2)) scaled to DD2 strength level with respect to Turkish seismic code provisions, corresponding to probability of exceedance of 10 % in 50 years (with return period of 475 years). The

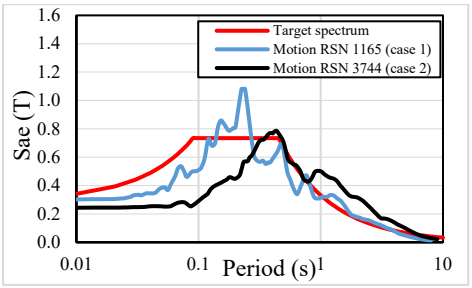

Fig. 8 Response spectra of the two example motions scaled to the target spectrum

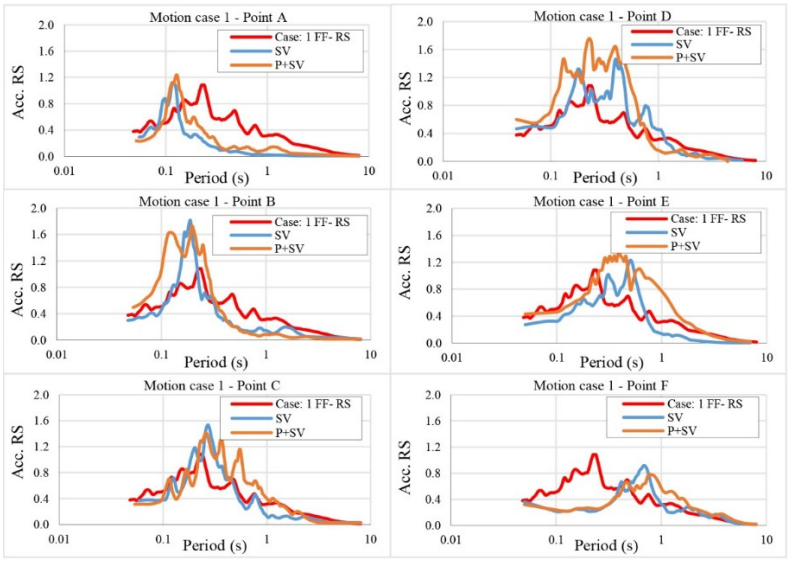

Fig. 9 Acceleration response spectra at the soft clayey basin surface for the motion case 1 (basin depth: 50 m)

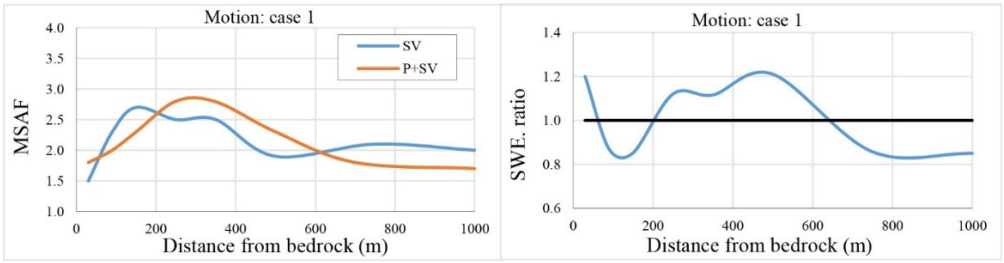

Fig. 10 Variation of the MSAF (left) and SWE (right) at the soft clayey basin surface for motion case 1 (basin depth: 50 m)

response of the 50m depth trapezoidal basin with soft clayey soil has been estimated by the applied fully nonlinear method under P+SV and SV wave incident conditions.

Fig. 9 presents the acceleration response spectra at different points of the basin surface for the selected example motion case 1 at half width of the basin. It shows the variation of the basin response at different surface points. As can be seen, while the maximum response at points close to the bedrock outcrop happens at lower period (points A, B and C), it occurs at the higher period at inner parts of the basin (points D, E and F). But, the important point is the difference between the period of the SV and P+SV maximum responses over basin surface. It happens because of the reflection and refraction of the bedrock motion at basin edge as well as the generation of the progressive surface waves. It in turn, affects the spectral amplification with respect to the free-field condition. The change in the period of the maximum surface response to different incident waves is evident at some of the points. To make these results more meaningful, the variation of the maximum spectral amplification factor (MSAF) for this case is presented in Fig. 10. It is seen that the effect of the P+SV incident wave is greater over 400 m of the basin surface (about 40% of the basin). Also, the SWE ratio reaches to about 20% in this area. The effect was investigated for another example motion (motion case 2) with frequency content different from motion case 1. Fig. 11 shows the variation of the basin response at different surface points under the effect of motion case 2. For this

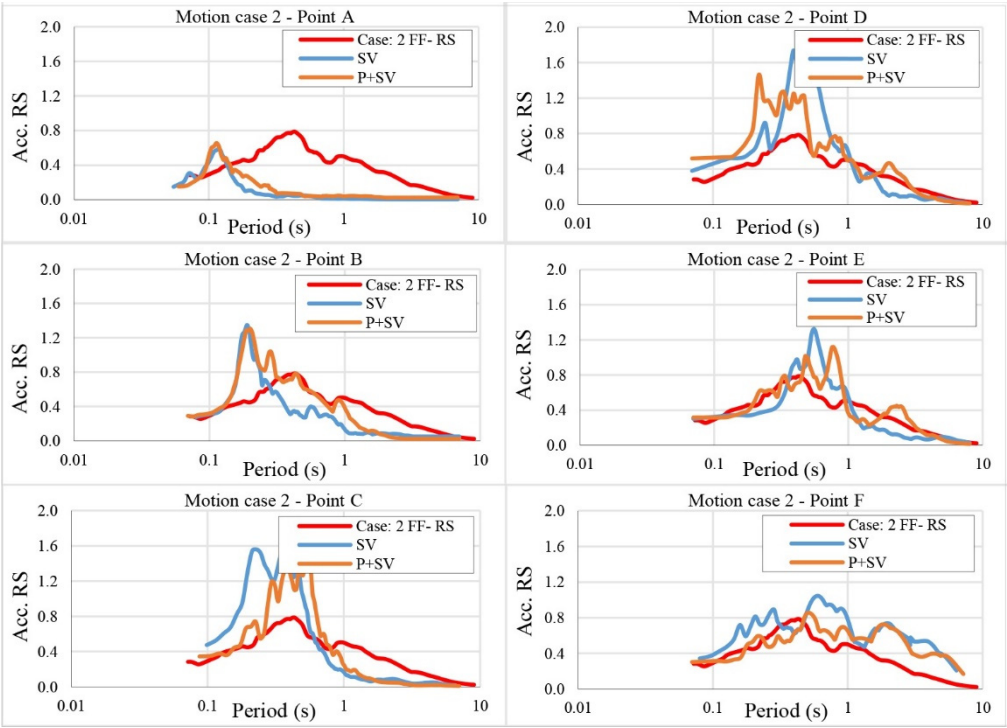

Fig. 11 Acceleration response spectra at the soft clayey basin surface for the motion case 2 (basin depth: 50 m)

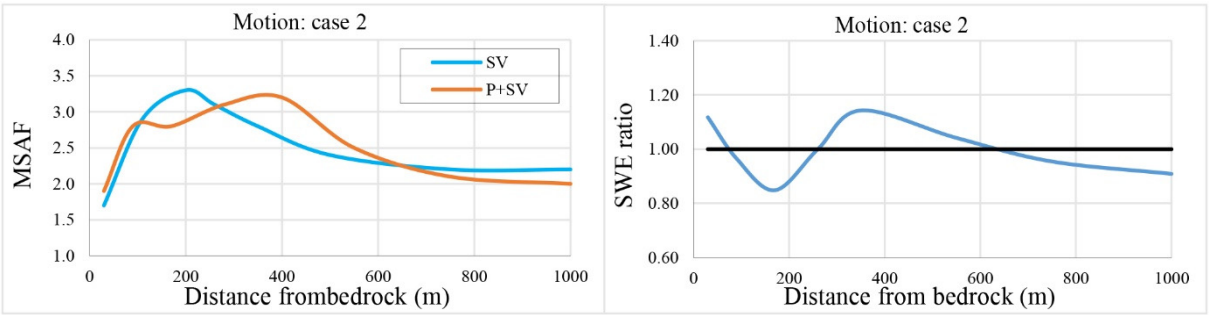

Fig. 12 Variation of the MSAF (left) and SWE (right) at the soft clayey basin surface for motion case 2 (basin depth: 50 m)

case, the change in the period of the maximum response is more evident especially at points C, D and E. Using these data, the variation of the MSAF can be estimated for this case. Fig. 12 shows that the greater effect of the P+SV incident wave exist over 350 m for this case (about 35% of the basin). Finally, the estimated SWE ratio indicates the 15% effect of the P+SV incident wave for this case. It is worth noting that, in addition to the aggravating effect, the simultaneous application of the P+SV incident waves has got suppressive effect, too. This effect and its influence range can also be seen in SWE ratio figures.

Since earthquakes are random motions identified by several parameters, to consider the effects of these parameters, as well as to remove the motion dependency of the results, the average response of the trapezoidal soft clayey basin with 50m depth and basin edge inclination of 10° to the collection of 24 strong ground motions (Table 2) scaled to the DD2 strength level with respect to Turkish seismic code are estimated. Fig. 13 shows the variation of the MSAF at the basin surface under the effect of the SV and P+SV incident motions at half width of the basin. It is seen that there is an about 500 m aggravating effect zone between two suppressive zones. While the MSAF of the P+SV condition exceeds SV condition at the basin edge, it remains less than SV condition at the basin center. Also. SWE ratio reaches up to about 18%. The suppressive effect at the area close to the bedrock outcrop and basin center remains about 10%.

3.2 Effect of ground stiffness

To see the effect of the change in the soil type, response of the stiff clayey basin to P+SV and SV incident waves under the effect of the collection of 24 strong ground motions (50 m depth and 10° of basin edge inclination) are presented in Fig. 14.

The results show that the 2D basin edge effect has remained limited to almost 500 m from the bedrock outcrop for both incident waves conditions. The greater effect of the P+SV conditions over 250 m of the basin half width is

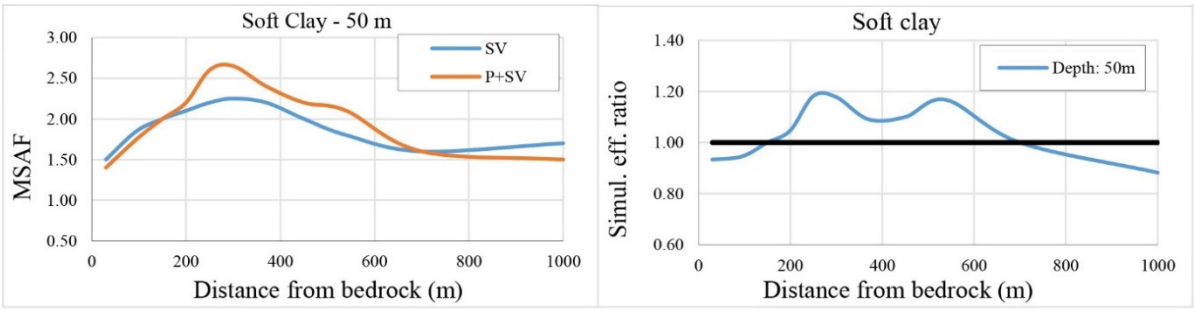

Fig. 13 Variation of the MSAF (left) and SWE (right) at the soft clayey basin surface averaged over 24 motions scaled to the target spectrum (basin depth: 50 m)

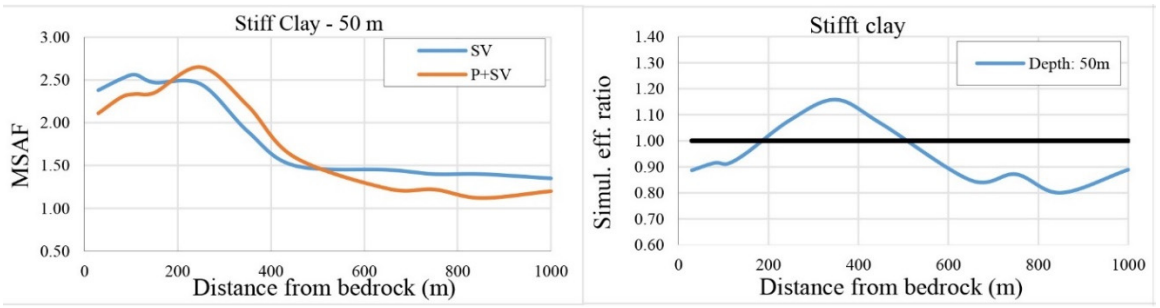

Fig. 14 Variation of the MSAF (left) and SWE (right) at the stiff clayey basin surface averaged over 24 motions scaled to the target spectrum (basin depth: 50 m)

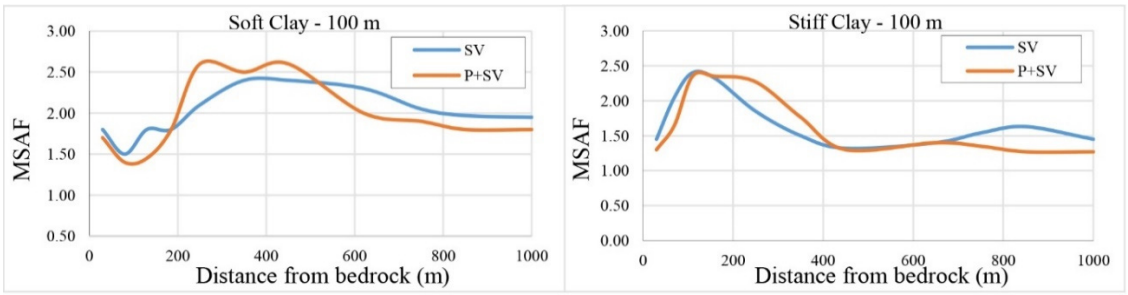

Fig. 15 Variation of the MSAF (left) and SWE (right) at the soft clayey basin surface averaged over 24 motions scaled to the target spectrum (basin depth: 100 m)

evident. Also, the SWE ratio reaches to about 15% and 20% for aggravating and suppressive conditions, respectively.

3.3 Effect of the basin depth

Generally, basins with the depth of 100 m are considered as the shallow basins (Semblat *et al*. 2002, Zhu *et al.* 2018, Khanbabazadeh 2024). In this section, to see the effect of the basin depth, response of the both soft and stiff clayey basins (100 m depth and 10° of basin edge inclination) are investigated.

Fig. 15 shows that while almost 800 m of the basin surface has been influenced by the edge effect at soft clayey basin, it is limited to about 400m at stiff clayey basin. At both basins, the maximums of the responses have been happened under the effect of the P+SV incident waves. Towards the basin center, the effect of the SV incident waves are greater. The effect of these behaviors is also reflected in the SWE ratio curves in Fig. 16. Unlike the different influence range for soft and stiff clayey basins, their maximum SWE ratio are about 23% for both incident wave conditions. Also, compared to the shallower 50 m depth basin, the greater effect of the P+SV incident wave at 100 m depth basins are concluded. The effect of the change in soil stiffness can also be seen in this figure. In soft clayey soils with lower natural frequency with respect to the stiff clayey soils, the interaction between body waves at the basin edges gives rise to the generation of the surface waves progressing towards the basin center. As a result, the maximums of the MSAF happen in the region away from the basin edge. On the other hand, trapping of the waves with higher frequency in the edges of the stiff clayey basin results in greater MSAF in this region.

4. Conclusions

For consideration of the 2D/3D topographic effects in design spectrum estimation, earthquake design codes instruct the use of the horizontal components of the

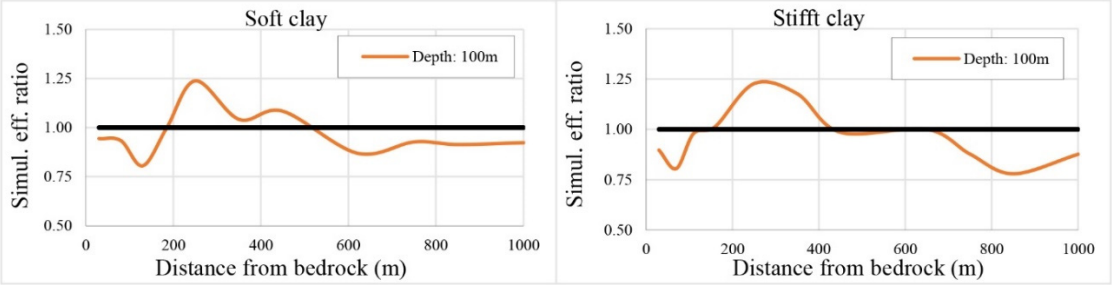

Fig. 16 Variation of the MSAF (left) and SWE (right) at the stiff clayey basin surface averaged over 24 motions scaled to the target spectrum (basin depth: 100 m)

motions. Nevertheless, the aggravating effect of the P and SV waves due to the refraction of the incident P wave component from inclined basin edge is neglected. Although this approximation remains conservative for horizontal bedrock conditions, its effect at basins with 2D/3D bedrock geometry would be of importance. Also, the difficulties of the simultaneous application of the P and SV components in the time domain is another reason of such approximation. The major contribution of this study is to present a quantitative ratio in terms of amplification factor for comparison between the simultaneous P+SV and only SV incident wave condition. To attain this goal, an advanced numerical modeling scheme capable of simultaneously modeling of the P and SV incident motions in time domain was applied. As a result, the effect of the parameters such as mixing and interference of different frequency components, frequency independent hysteresis damping as well as nonlinear behavior of the soil are reflected in the results.

The results showed the effect of the P+SV cases on the frequency content of the basin response with respect to the only SV case. The effect is generally more noticeable at middle part (between the zone close to the outcrop and basin center). While the P+SV aggravating effect reached to about 18% at soft clayey basin with 50 m depth, it reached to about 15% for the stiff clayey basin. By the change in the clay type from soft to stiff, the aggravating effect length decreases from 500 m to the 250 m, respectively. Also, the effect of the basin depth was investigated in this study. It was seen that for both soft and stiff clayey basins with 100m depth, the P+SV aggravating effect reaches to close values of about 25%. Nevertheless, the aggravating effect length for 100 m depth basin is shorter with respect to the shallower 50 m depth case.

Also, the results of this study showed the suppressive effect of the P+SV incident condition at some parts of the basin surface as well. It was seen that the suppressive effect of the P+SV incident condition holds true for the basin central part that the 1D behavior is dormant. It is concluded that the application of only SV incident wave is 10% to 20% conservative for different clay types and basin depth conditions.

References

Abraham, J.R., Lai, C.G. and Papageorgiou, A. (2015), "Basin-effects observed during the 2012 Emilia earthquake sequence in Northern Italy", *Soil Dyn. Earthq. Eng.*, **78**, 230-242. https://doi.org/10.1016/j.soildyn.2015.08.007.

Alielahi, H. and Adampira, M. (2017), "Evaluation of 2D seismic site response due to hill-cavity interaction using boundary element technique", *J. Earthq. Eng.*, **22**(6), 1137-1167. https://doi.org/10.1080/13632469.2016.1277437.

Alielahi, H. and Rahimi, M. (2025), "A study on 1D and 2D seismic site response analysis in a complex sedimentary basin: A case study", *Soil Dyn. Indian Geotech. J.*, 1-22. https://doi.org/10.1007/s40098-025-01407-z.

Anbazhagan, P., Aditya, P. and Rashmi, H.N. (2011), "Amplification based on shear wave velocity for seismic zonation: comparison of empirical relations and site response results for shallow engineering bedrock sites", *Geomech. Eng.*, **3**(3), 189-206. https://doi.org/10.12989/gae.2011.3.3.189.

Ayoubi, P., Mohammadi, K. and Asimaki, D. (2021), "A systematic analysis of basin effects on surface ground motion", *Soil Dyn. Eearthq. Eng.*, **141**, 106490. https://doi.org/10.1016/j.soildyn.2020.106490.

Ba, Z., Wang, Y., Liang, J. and Lee, V.W. (2020), "Wave scattering of plane P, SV, and SH waves by a 3D alluvial basin in a multilayered half-space", *Bull. Seismol. Soc. Am.*, **110**(2), 576-595. https://doi.org/10.1785/0120190090.

Bakir, B.S., Ozkan, M.Y. and Ciliz, S. (2002), "Effects of basin edge on the distribution of damage in 1995 Dinar, Turkey earthquake", *Soil Dyn. Earthq. Eng.*, **22**, 335-345. https://doi.org/10.1016/S0267-7261(02)00015-5.

Bordoni P., Gori S., Akinci A., Visini F., Sgobba S., Pacor F., Cara F., Pampanin S., Milana G. and Doglioni C. (2023), "A site-specific earthquake ground response analysis using a fault-based approach and nonlinear modeling: The Case Pente site (Sulmona, Italy)", *Eng Geol.*, **314**, 106970, https://doi.org/10.1016/j.enggeo.2022.106970.

Cao, S. and Greenhalgh, S. (1992), "Finite-difference simulation of P-S V-wave propagation: A displacement-potential approach", *Geophys. J. Int.*, **109**(3), 525-535. https://doi.org/10.1111/j.1365-246X.1992.tb00115x.

Cundall, P.A. (2016), "FLAC3D manual: A computer program for fast lagrangian analysis of continua (Version 6.0)", Minneapolis Uni., MN, USA.

Gil-Zepeda, S.A., Montalvo-Arrieta, J.C., Vai, R. and Sanchez-Sesma, F.J. (2003), "A hybrid indirect boundary element discrete wave number method applied to simulate the seismic response of stratified alluvial valleys", *Soil Dyn. Earthq. Eng.*, **23**, 77-86. https://doi.org/10.1016/S0267-7261(02)00092-1.

Griffiths, S., Cox, B. and Rathje, E. (2016), "Challenges associated with site response analyses for soft soils subjected to high-intensity input ground motions", *Soil Dyn. Earthq. Eng.*, **85**, 1-10, https://doi.org/10.1016/j.soildyn.2016.03.008.

Hasal, M.E., Iyisan, R. and Yamanaka, H. (2018), "Basin edge effect on seismic ground response: a parametric study for Duzce basin case, Turkey", *Arabian J. Sci. Eng.*, **43**, 2069-2081.

https://doi.org/10.1007/s13369-017-2971-7.

Iyisan, R. and Khanbabazadeh, H. (2013), "A numerical study on the basin edge effect on soil amplification", *Bull. Earthq. Eng.*, **11**, 1305-1323, https://doi.org/10.1007/s10518-013-9451-6.

Jakka, R.S., Hussain, M.D. and Sharma, M.L. (2015), "Effects on amplification of strong ground motion due to deep soils", *Geomech. Eng.*, **8**(5), 663-674. https://doi.org/10.12989/gae.2015.8.5.663.

Kamalian, M., Jafari, M.K, Sohrabi-Bidar, A., Razmkhah, A. and Gatmiri, B. (2006), "Time domain two-dimensional site response analysis of non-homogeneous topographic structures by a hybrid BE/FE method", *Soil Dyn. Earthq. Eng*., **26**, 753-765. https://doi.org/10.1016/j.soildyn.2005.12.008.

Kamiyama, M. and Satoh, T. (2002), "Seismic response analysis of laterally inhomogeneous ground with emphasis on strains", *Soil Dyn. Earthq. Eng*., **22**, 877-884. https://doi.org/10.1016/S0267-7261(02)00110-0.

Khanbabazadeh, H. (2024), "Nonlinearity effect on the dynamic behavior of the clayey basin edge", *Geomech. Eng.*, **36** (4), 367-380. https://doi.org/10.12989/gae.2024.36.4.367.

Khanbabazadeh, H. and Iyisan, R. (2014a), "A numerical study on the 2D behavior of clayey basins", *Soil Dyn. Earthq. Eng.*, **66**, 31-41. https://doi.org/10.1016/j.soildyn.2014.06.029.

Khanbabazadeh, H. and Iyisan, R. (2014b), "A numerical study on the 2D behavior of the single and layered clayey basins", *Bull. Earthq. Eng.*, **12**, 1515-1536. https://doi.org/10.1007/s10518-014-9590-4.

Khanbabazadeh, H., Iyisan, R., Ansal, A. and Hasal, M.E. (2016), "2D non-linear seismic response of the Dinar basin,Turkey", *Soil Dyn. Earthq. Eng.*, **89**, 5-11. https://doi.org/10.1016/j.soildyn.2016.07.021.

Khanbabazadeh, H., Hasal, M.E. and Iyisan, R. (2019), "2D seismic response of the Duzce Basin, Turkey", *Soil Dyn. Earthq. Eng.,* **125**, 105754. .https://doi.org/10.1016/j.soildyn.2019.105754.

Khanbabazadeh, H., Zulfikar, A.C. and Yesilyurt, A. (2020), "Basin edge effect on industrial structures damage pattern at clayeybasins", *Geomech. Eng.*, **23**(6), 575-585. https://doi.org/10.12989/gae.2020.23.6.575.

Khoshghalb, A., Shafee, A., Tootoonchi, A., Ghaffaripour, O. and Jazaeri, S.A. (2020), "Application of the smoothed point interpolation methods in computational geomechanics: A comparative study", *Comput. Geotech.*, **126**, 103714. https://doi.org/10.1016/j.compgeo.2020.103714.

Kumar, V., Narayan, J.P., Khatri, V., Kumar, N. and Kamal, (2021), "Effects of P-SV wave propagation on ground motion characteristics due to variation in subsurface basement topography", *J Ind. Geophys. Union.*, **25**(1), 1-8.

Liang, J., Wang Y., Ba, Z. and Zhong, H. (2021), "A special indirect boundary element method for seismic response of a 3D canyon in a saturated layered half-space subjected to obliquely incident plane waves", *Eng. Anal. Bound. Elem.*, **132**(1), 182-201. https://doi.org/10.1016/j.enganabound.2021.07.003.

Madiai, C., Facciorusso, J. and Gargini, E. (2017), "Numerical modeling of seismic site effects in a shallow alluvial basin of the northern Apennines (Italy)", *Bull. Seismol. Soc. Am.*, **107**, 2094-105. https://doi.org/10.1785/0120160293.

Makra, K. and Chavez-Garci, F.J. (2016), "Site effects in 3D basins using 1D and 2D models: an evaluation of the differences based on simulations of the seismic response of Euroseistest", *Bull. Earthq. Eng.*, **14,** 1177-1194. https://doi.org/10.1007/s10518-015-9862-7.

Makra, K., Chavez-Garcıa, F.J., Raptakis, D. and Pitilakis K. (2005), "Parametric analysis of the seismic response of a 2D sedimentary valley: Implications for code implementations of complex site effects", *Soil Dyn. Earthq. Eng.*, **25**, 303-315. https://doi.org/10.1016/j.soildyn.2005.02.003.

Madiai, C., Facciorusso, J., Gargini, E. and Baglione, M. (2016), "1D versus 2D site effects from numerical analyses on a cross section at Barberino di Mugello (Tuscany,Italy)", *Procedia Eng.*, **158**, 499-504. https://doi.org/10.1016/j.proeng.2016.08.479.

Manakou, M.V., Raptakis, D.G., Chavez-Garci, F.J., Apostolidis, P. I. and Pitilakis, K.D. (2010), "3D soil structure of the Mygdonian basin for site response analysis", *Soil Dyn. Earthq. Eng.*, **30**, 1198-1211. https://doi.org/10.1016/j.soildyn.2010.04.027.

Mayoral, J.M., Asimaki, D., Tepalcapa, S., Wood, C., Sancha, A.R., Hutchinson, T., Franke, K. and Montalva, G. (2019) "Site effects in Mexico City basin: past and present", *Soil Dyn. Earthq. Eng.*, **121**, 369-382. https://doi.org/10.1016/j.soildyn.2019.02.028.

Oral, E., Gelis, C. and Bonilla, F. (2023), "2-D P-SV and SH spectral element modelling of seismic wave propagation in non-linear media with pore-pressure effects", *Geophys. J. Int.*, **232**, 53-56. https://doi.org/10.1093/gji/ggac304.

Ozaslan, B., Iyisan, R., Hasal, M.E., Khanbabazadeh, H. and Yamanaka, H. (2022), "Assessment of the design spectrum with aggravation factors by 2D nonlinear numerical analyses: A case study in the Gemlik Basin, Turkey", *Bull. Earthq. Eng*., **20**(3), 1371-1395. https://doi.org/10.1007/s10518-021-01296-6.

Pitilakis, K. (2004), "Site effects", *Recent advances in earthquake geotechnical engineering and microzonation*, **1.** Netherlands: Kluwer Academic Publishers.

Rodriguez-Plata, R., Ozcebe, A.G., Smerzini, C. and Lai, C.G. (2021), "Aggravation factors for 2D site effects in sedimentary basins: The case of Norcia, central Italy*", Soil Dyn. Earthq. Eng.*, **149**, 106854. https://doi.org/10.1016/j.soildyn.2021.106854.

Roy, N. and Sahu, R.B. (2012), "Site specific ground motion simulation and seismic response analysis for microzonation of Kolkata", *Geomech. Eng.*, **4**(1), 1-18. https://doi.org/10.12989/gae.2012.4.1.001.

Saenz, M., Sierra, C., Vergara, J., Jaramillo, J. and Gomez, J. (2019), "Site specific analysis using topography conditioned response spectra", *Soil Dyn. Earthq. Eng.*, **123**, 470-497. https://doi.org/10.1016/j.soildyn.2019.03.004.

Saffarian, M.A. and Bagheripour, M.H. (2014), "Seismic response analysis of layered soils considering effect of surcharge mass using HFTD approach. Part I: Basic formulation and linear HFTD", *Geomech. Eng*., **6**(6), 517-530. https://doi.org/10.12989/gae.2014.6.6.517.

Salehi Dezfooli, M., Khoshghalb, A. and Shafee, A. (2022), "An automatic adaptive edge-based smoothed point interpolation method for coupled flow-deformation analysis of saturated porous media", *Comput. Geotech.*, **145**, 104672. https://doi.org/10.1016/j.compgeo.2022.104672.

Semblat, J.F. (2011), "Modeling seismic wave propagation and amplification in 1D/2D/3D linear and nonlinear unbounded media", *Int. J. Geomech.*, **11**(6), 440-448. https://doi.org/10.1061/(ASCE)GM.1943-5622.0000023.

Semblat, J.F., Dangla, P., Khama, M. and Duva, A.M. (2002), "Seismic site effects for shallow and deep alluvial basins: in-depth motion and focusing effect", *Soil Dyn. Earthq. Eng.*, **22**, 849-854. https://doi.org/10.1016/S0267-7261(02)00107-0.

Semblat, J.F., Duval, A.M. and Dangla, P. (2000), "Numerical analysis of seismic wave amplification in Nice (France) and comparisons with experiments", *Soil Dyn. Earthq. Eng.*, **19**(5), 347-362. https://doi.org/10.1016/S0267-7261(00)00016-6.

Shafee, A. and Khoshghalb, A. (2021), "An improved node-based smoothed point interpolation method for coupled hydro-mechanical problems in geomechanics", *Comput. Geotech.*, **139**, 104415. https://doi.org/10.1016/j.compgeo.2021.104415.

Shafee, A. and Khoshghalb, A. (2022), "Particle node-based

smoothed point interpolation method with stress regularisation for large deformation problems in geomechanics", *Comput. Geotech.*, **141**, 104494. https://doi.org/10.1016/j.compgeo.2021.104494.

Shani-Kadmiel S., Tsesarsky M., Louie J. N., Gvirtzman Z. (2012), "Simulation of seismic-wave propagation through geometrically complex basins: The Dead Sea Basin", *Bull. Seismol. Soc. Am.*, **102**(4), 1729-1739. https://doi.org/10.1785/0120110254.

Shiuly, A., Sahu, R.B. and Mandal, S. (2015), "Seismic microzonation of Kolkata", *Geomech. Eng.*, **9**(2), 125-144. https://doi.org/10.12989/gae.2015.9.2.125.

Silahtar, A. and Kanbur, M.Z. (2021), "1D nonlinear site response analysis of the Isparta Basin (Southwestern Turkey) with surface wave (ReMi) and borehole data", *Environ. Earth Sci.*, **80**, 268. https://doi.org/10.1007/s12665-021-09551-4.

Sonmezer, Y.B., Bas, S., Isik, N.S. and Akbas, S.O. (2018), "Linear and nonlinear site response analyses to determine dynamic soil properties of Kirikkale", *Geomech. Eng.*, **16**(4), 435-448. https://doi.org/10.12989/gae.2018.16.4.435.

Sonmezer, Y.B. and Celiker, M. (2020), "Determination of seismic hazard and soil response of a critical region in Turkey considering far-field and near-field earthquake effect", *Geomech. Eng.*, **20**(2), 131-146. https://doi.org/10.12989/gae.2020.20.2.131.

Sreejava, K.P., Raghukanth, S.T.G. and Srinagesh, D.M. (2023), "Seismic wave propagation simulations in Indo-Gangetic basin using spectral element method", *Geophys. J. Int*., **232**, 247-273. https://doi.org/10.1093/gji/ggac301.

Stamati, O., Klimis, N. and Lazaridis, T. (2016), "Evidence of complex site effect sand soil non-linearity numerically estimated by 2D vs 1D seismic response analyses in the city of Xanthi", *Soil Dyn. Earthq. Eng.*, **87**, 101-115. https://doi.org/10.1016/j.soildyn.2016.05.006.

Stanko, D., Gulerce, Z., Markusic, S. and Salic, R. (2019), "Evaluation of the site amplification factors estimated by equivalent linear site response analysis using time series and random vibration theory based approaches", *Soil Dyn. Earthq. Eng.*, **117**, 16-29. https://doi.org/10.1016/j.soildyn.2018.11.007.

Vireux, J. (1986), "P-SV wave propagation in heterogeneous media: Velocity-stress finite-difference method", *Geophysics*, **51**(4), 889-1033. https://doi.org/10.1190/1.1442147.

Yniesta, S., Brandenberg, S.J. and Shafiee, A. (2017), "ARCS: A one dimensional nonlinear soil model for ground response analysis", *Soil Dyn. Earthq. Eng.*, **102**, 75-85. https://doi.org/10.1016/j.soildyn.2017.08.015.

Zhu, C., Chavez-Garcia, F.J., Thambiratnam, D. and Gallage, C. (2018), "Quantifying the edge-induced seismic aggravation in shallow basins relative to the 1D SH model", *Soil Dyn. Earthq. Eng.*, **115**, 402-412. https://doi.org/10.1016/j.soildyn.2018.08.025.

Zhu, C. and Thambiratnam, D. (2016), "Interaction of geometry and mechanical property of trapezoidal sedimentary basins with incident SH waves", *Bull. Earthq. Eng.*, **14**, 2977-3002. https://doi.org/10.1007/s10518-016-9938-z.